Indium Oxide with Novel Morphology: Synthesis and Application in C 2 H 5 OH Gas Sensing

ARTICLE *in* CRYSTAL GROWTH & DESIGN · MAY 2009

Impact Factor: 4.89 · DOI: 10.1021/cg8007238

6 AUTHORS, INCLUDING:

Jiaqiang Xu
Shanghai University
144 PUBLICATIONS **3,753** CITATIONS

Article

Indium Oxide with Novel Morphology: Synthesis and Application in CHOH Gas Sensing

E. Li, Zhixuan Cheng, Jiaqiang Xu, Qingyi Pan, Weijun Yu, and Yuliang Chu

Cryst. Growth Des., **2009**, 9 (5), 2146-2151• Publication Date (Web): 26 March 2009

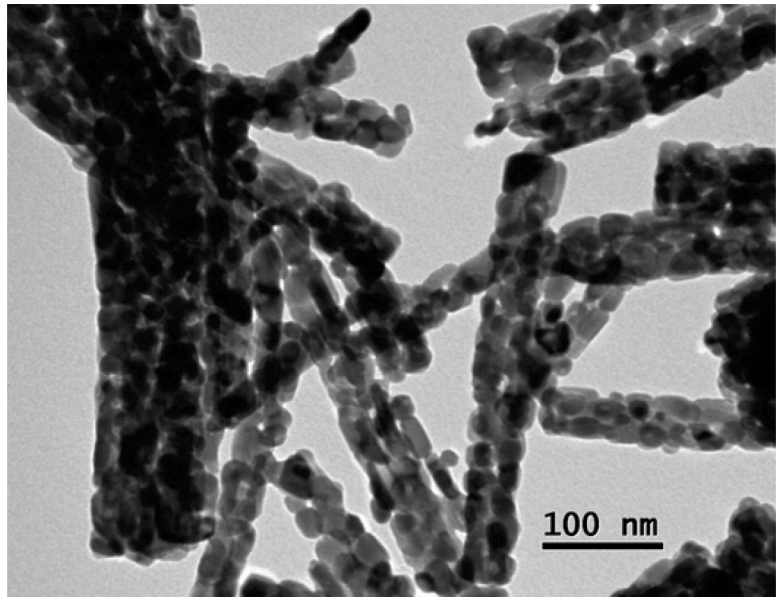

CRYSTAL GROWTH & DESIGN
2009
VOL. 9, NO. 5
2146–2151

Indium Oxide with Novel Morphology: Synthesis and Application in C_2H_5OH Gas Sensing

E. Li,[†] Zhixuan Cheng,*[,†] Jiaqiang Xu,[†] Qingyi Pan,[†] Weijun Yu,[‡] and Yuliang Chu[‡]

Department of Chemistry, College of Science, Shanghai University, Shanghai 200444, PR China, and Instrumental Analysis and Research Center, Shanghai University, Shanghai 200444, PR China

Received July 7, 2008; Revised Manuscript Received February 23, 2009

ABSTRACT: In this work, mesoporous In_2O_3 nanorods composed of many small well-aligned crystal nanostructures have been fabricated by a simple sol−gel process, with block copolymer PE6800 as a soft template controlling their morphology. The effects of the experimental parameters such as the concentration of PE6800, the dosage of $InCl_3 \cdot 4H_2O$, reaction temperature, and pH values were investigated by a series of experiments. The as-synthesized mesoporous In_2O_3 nanorods showed excellent gas-sensing properties to C_2H_5OH in terms of sensor response and selectivity.

1. Introduction

Since the scientists at Mobil Corporation reported their pioneering work on silica-based mesoporous materials in 1992,[1] mesoporous materials have attracted intensive attention for enormous mesopores, nanometer characteristics, and potential applications in molecular separation,[2] heterogeneous catalysis,[3] nanocomposite preparation,[4,5] and gas sensors.[6,7] At present many methods have been used to prepare mesoporous materials. In general, mesoporous oxide materials synthesis requires structural templates. The most hydrothermal synthesis methods use soft templates, such as surfactants,[8,9] while other methods use hard templates such as porous alumina[10] or silica.[11]

The fabrication of one-dimensional (1D), nanoscale building blocks such as nanowires, nanorods, nanobelts, and nanotubes have been researched intensively because of their potential applications in mesoscopic physics and fabrication of nanoscale devices.[12,13] To this aim, various techniques including arcdischarge, laser ablation, template, precursor thermal decomposition have been developed to prepare well-aligned nanowires/nanorods.[14−17] However, it is still a challenge to develop simple methods to fabricate uniform nanorods that are cost-effective and allow large-scale production.

Indium oxide, an important transparent conductive oxide (TCO) with a wide band gap close to GaN (3.5−3.7 eV), has been well studied in past years because of its excellent properties in application such as solar cells,[18] flat-panel displays,[19] solid-state optoelectronic devices,[20] and gas sensors.[21] As the morphology of nanomaterials is one of the key factors that affects their properties, the nanostructures with novel morphologies have been investigated. In recent years, various morphological nanostructures of In_2O_3, for instance, nanocrystals,[22,23] nanowires,[24] nanorods,[25,26] and nonobelts[27] have been reported in the literature. A variety of chemical methods have been demonstrated to prepare 1D nanostructures of In_2O_3. Most of them involved hydrothermal (or solvothermal) processes under elevated pressures and temperatures. In comparison, the sol−gel method could be performed under the ambient pressure and with conventional glassware.

Many researchers reported that In_2O_3 was a promising material for detection of low concentrations of oxidizing gases like O_3,[28,29] NO_2[30,31] and reducing gases like CO,[32] H_2.[33] But the reponse of pure In_2O_3 sensor to C_2H_5OH was lower. The response to 100 ppm C_2H_5OH was less than 3 based on pure In_2O_3 nanowires sensors.[34]

In this paper, a simple sol−gel technique was applied to prepare mesoporous In_2O_3 nanorods consisting of interconnected nanocrystallites of ∼20 nm in size. Mesoporous In_2O_3 nanorods composed of many small well-aligned crystal nanostructures could be first readily synthesized using a simple sol−gel process. The gas sensitivity results show that mesoporous In_2O_3 nanorods are very sensitive to dilute ethanol. It can detect 500 ppb C_2H_5OH at about 290 °C with a reponse value of 1.71, the response and the recovery time are 6 and 8 s, respectively. The response intensity of mesoporous In_2O_3 nanorods to 100 ppm C_2H_5OH is 8.43, which is higher than that of pure In_2O_3 nanowire sensors.

2. Experimental Section

All the reagents (analytical-grade purity) were purchased from Shanghai Chemical Reagent Co. Ltd. (Shanghai, China), except for amphiphilic triblock copolymer PE6800, poly(ethylene oxide)-poly(propylene oxide)-poly(ethylene oxide) ($EO_{73}-PO_{28}-EO_{73}$, $M_w = 8050$), obtained from BASF, and used without further purification.

2.1. Synthesis. In a typical synthesis, 1.0 g of surfactant (PE6800) was dissolved into 100 mL of deionized water, 0.01 mol of $InCl_3 \cdot 4H_2O$ was then added into the solution, and ammonia was diluted with deionized water to a concentration of 1 mol/L. Then the ammonia diluted was dropped into the $InCl_3$ solution with continuous stirring at 60 °C in a water bath, and the pH value of the final solution was controlled at 6.4. After aging for 24 h, the precipitate was poured out into a tube for centrifugal separating, and washed with deionized water until no chloride ions were detected in the filtrate. Then the products were aged in air at 60 °C for 24 h. The yellow indium oxide powders were obtained by calcining at 500 °C for 2 h to remove the surfactant. To investigate the morphological evolution of the 1D nanomaterials, some samples were obtained under different preparation conditions, such as the temperature, the quantities of PE6800, the dosage of $InCl_3 \cdot 4H_2O$, and the pH values. The detailed experimental parameters are listed in Table 1.

2.2. Characterization. Morphologies and sizes of the samples were characterized by transmission electron microscopy (TEM, JEOL JEM-200CX working at 160 kV; JEOL JEM 2010F operated at 200 kV) and field emission scaning electron microscopy (FE-SEM, JEOL JSM-6700F operated at 15 kV). Crystal structure of the as-prepared products was identified by powder X-ray diffraction (XRD) analysis using a D/max 2550 V diffractometer with Cu Kα radiation ($\lambda = 1.54056$ Å) (Rigaku, Tokyo, Japan), and the XRD data were collected at a scanning rate of 0.02 ° s^{-1} for 2θ in a range of 10°−70°. The decomposition

* Corresponding author. Tel: +86 21 66132927. E-mail: zxcheng@staff.shu.edu.cn.
[†] Department of Chemistry, College of Science.
[‡] Instrumental Analysis and Research Center.

10.1021/cg8007238 CCC: $40.75
Published on Web 03/26/2009

Table 1. In_2O_3 Morphologies, Synthesis Parameters

synthesis parameters				
PE6800 (g)	temperature (°C)	$InCl_3 \cdot 4H_2O$ (mol)	pH	morphologies
0.0	60	0.010	6.4	nanoparticles
0.5	60	0.010	6.4	nanorods
1.0	60	0.010	6.4	nanorods with pores
1.5	60	0.010	6.4	nanorods
1.0	25	0.010	6.4	nanoparticles with pores
1.0	40	0.010	6.4	nanorods and nanospheres
1.0	80	0.010	6.4	shorter nanorods bundles
1.0	60	0.005	6.4	shorter nanorods
1.0	60	0.015	6.4	shorter and thicker nanorods
1.0	60	0.010	5.0	nanorods with no pores
1.0	60	0.010	7.5	nanorods and agglomerated

process of the $In(OH)_3$ precursor was investigated on a STA409PC thermal analyzer (Netzsch, Germany) with a heating rate of 10 °C min^{-1} under an air atmosphere.

2.3. Gas-Sensing Properties Research. The final powders were mixed and ground with an adhesive in an agate mortar to form a gas-sensing paste. The paste was coated onto an alumina tube on which a pair of Au electrodes was previously printed, then dried under IR radiation for several minutes in air, and subsequently sintered at 500 °C for 2 h. Finally, the electrodes were jointed on a base and a Ni−Cr heating wire was inserted. The gas sensors were aged at 300 °C for 7 days in order to improve their stability. The gas response was measured in the static state. The gases to be tested were injected into a test bottle and mixed with air. Figure 1 shows a schematic drawing of gas sensor. The measuring electric circuit for the gas sensor is shown in Figure 2. The working temperature of the sensors was adjusted by varying the heating voltage (V_h). By monitoring output voltage (V_{out}), the resistance of the sensor in air or test gas can be measured. Output voltage (V_{out}) is the terminal voltage of the load resistor. The response time is defined as the time required for the sample variation conductance to reach 90% of the equilibrium value following an injection of the test gas, and the recovery time is the time necessary for the sample to return to 10% above the original conductance in air after releasing the test gas. In this paper, the gas response of the sensor is defined as $S = R_g/R_a$, where R_g and R_a are the resistance of the sensors in the testing gas/air mixture and in air, respectively.

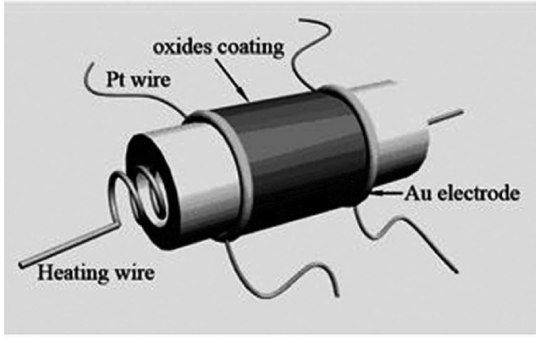

Figure 1. Sketch of the gas-sensor structure.

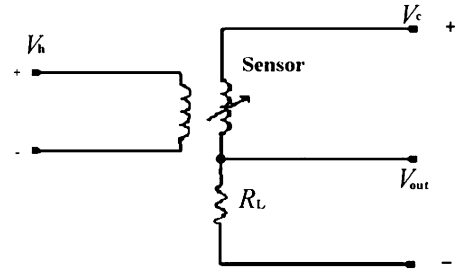

Figure 2. The measuring electric circuit of gas sensor.

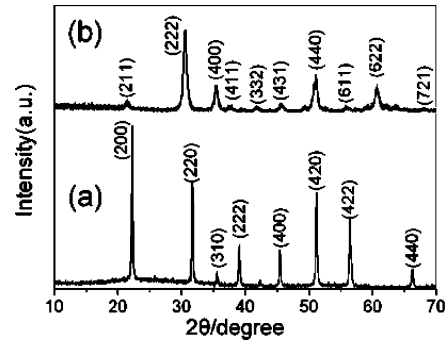

Figure 3. XRD patterns of $In(OH)_3$ nanorods (a) and mesoporous In_2O_3 nanorods (b).

3. Results and Discussion

3.1. Crystal Structure and Morphology. Crystal structure of the precursor and final In_2O_3 samples were characterized by X-ray diffraction (XRD). Figure 3a shows a XRD pattern of the precursor; all the diffraction peaks could be easily indexed to the body-centered cubic structure of $In(OH)_3$ (JCPDS card no. 16-0161, space group $Pn\bar{3}m$ (224), $a = 0.7958$ nm) with perfect crystallization. The XRD pattern of $In(OH)_3$ also showed that the ratio between the intensities of (200) diffraction lines and other diffraction lines was larger than the value in JCPDS card. The results indicated that the $In(OH)_3$ nanorods grew along the <100> directions.[35] The XRD pattern of the final products after sintering was also shown in Figure 3b. It showed that the powder was cubic In_2O_3. All the diffraction peaks completely agreed with those of JCPDS card No. 06-0416, space group $Ia3$ (206), $a = 1.011$ nm. No impure peaks were observed in the XRD pattern, indicating high purity of the sample.

Figure 4a,c shows the TEM micrograph of $In(OH)_3$ nanorods and mesoporous In_2O_3 nanorods. As shown in Figure 4a the as-prepared $In(OH)_3$ nanorods have a diameter of about 40 nm and a length of about 480 nm. The $In(OH)_3$ converted to In_2O_3 with controllable compositions and phase structures while maintaining the nanorods morphology after calcinations at 500 °C for 2 h in air (Figure 4a,c). The results showed that the rodlike morphology was completely preserved in the calcination process. However, each nanorod had been transformed from a dense structure with a smooth surface into a highly porous structure consisting of smaller nanoparticles. A TEM image showed that those nanoparticles were grown to an average diameter of 20 nm with a narrow size distribution (Figure 6a; the size distribution of the particles was measured from TEM images with at least 500 particles). So the pores were formed after the $In(OH)_3$ nanorods were calcined at 500 °C for 2 h. The relatively smooth surfaces of the $In(OH)_3$ had been significantly roughened after calcined at 500 °C. A closer examination of the TEM and SEM images indicates that some of the In_2O_3 nanorods might have aggregated into bundles. As shown in Figure 4b,c, the In_2O_3 nanorods surfaces are quite rough, possibly owing to a self-assembly mechanism in which smaller nanoparticles congregate into nanorods. This is a quite common phenomenon in self-assembly processes.[36]

The HRTEM image (Figure 4d) clearly indicates that In_2O_3 nanorods are polycrystalline structures and the small nanoparticles have clear lattice fringes with a lattice spacing of 0.29 nm, corresponding to the spacing of the (222) plane of *bcc* In_2O_3 crystal. The inset in Figure 4d is the corresponding SAED pattern, which clarifies that the diffraction spots can be indexed to the (222), (440) crystalline facets.

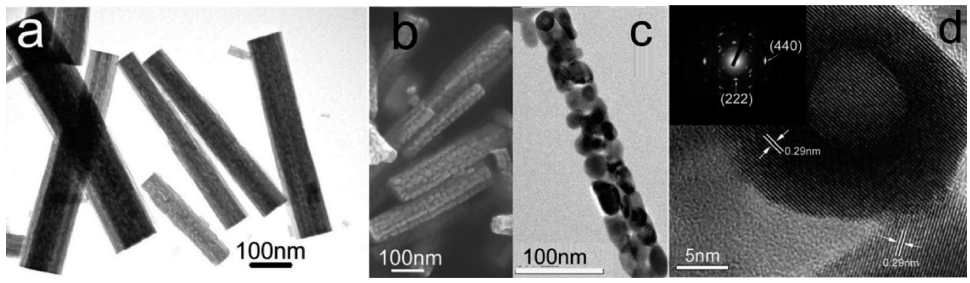

Figure 4. (a) TEM image of the $In(OH)_3$; (b) SEM image of the porous In_2O_3 nanorods at low magnification; (c) TEM image of the porous In_2O_3 nanorods at high magnification; (d) HRTEM of the mesoporous In_2O_3 nanorods. Inset is the corresponding SAED pattern.

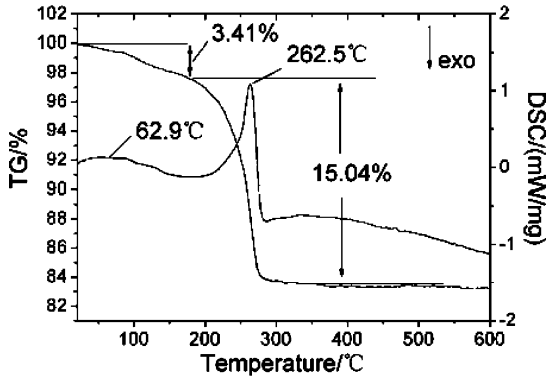

Figure 5. TG−DSC curve of the precursor of In_2O_3.

3.2. Thermal Analysis of the Precursor of In_2O_3. The thermal decomposition behavior of the precursor was studied using thermogravimetric−differential scanning calorimetry (TG−DSC). The TG-DSC curves of In_2O_3 precursor were shown in Figure 5. As shown in Figure 5, there are two endothermic peaks in the DSC curve. One is weak endothermic peak nearby 80 °C and the other is strong endothermic peak nearby 262 °C. Correspondingly, the TG curve shows that the weight loss occurs in two steps. One is a slow loss weight about 3.41% which may be absorption water lost and the remnant surfactant decomposition. The other is the strong loss of weight of about 15.04%. The observed weight loss of 15.04% was close to the calculated loss of 16.28%. According to this, we could conclude that the precursor completely decomposed above 262.5 °C in one step to form In_2O_3. The TG-DSC analysis and XRD results confirmed the complete decomposition of the precursor $In(OH)_3$ to In_2O_3.

3.3. Influencing Factors. The quantities PE6800, the reaction temperature, dosage of $InCl_3$ and pH are the main factors affecting formation of mesoporous In_2O_3 nanorods. Table 1 shows the reaction conditions for as-synthesized In_2O_3 with different morphologies.

Influence of PE6800 on the Morphology. Different quantities of PE6800 were used in the preparation to investigate the influence of PE6800. The sample was composed of irregular particles and serious agglomeration when no PE6800 was utilized in the reaction. When 0.5 g of PE6800 was utilized in the reaction, the sample mainly showed rod shapes with a width of about 100 nm and a length of about 500 nm, and the size of the smaller nanoparticles was about 16 nm, which was smaller than that of the smaller nanoparticles prepared with 1.0 g of PE6800 (Figure 6b). The pores in the In_2O_3 nanorods were not visible and the smaller nanoparticles were irregularly arranged; the size of the smaller nanoparticles was small compared with the sample prepared with 1.0 g of PE6800 (Figure 6a). When 1.5 g of PE6800 was added into the reaction system, the products were also In_2O_3 nanorods with pores and the size of the smaller nanoparticles was about 29 nm, which was bigger than that of the smaller nanoparticles prepared with 1.0 g of PE6800. Therefore, the surfactant PE6800 actually played an important role in controlling the morphology of In_2O_3 nanorods in the preparation process.

Influence of the Reaction Temperature on the Architecture. The morphology of the products was strongly affected by the reaction temperature. In order to study the effect of reaction temperature on the morphology of the final products, the reaction temperature varied from 25 to 80 °C. Figure 7 presents the TEM micrographs of In_2O_3 at different reaction temperatures. The morphology of the In_2O_3 prepared at 25 °C is porous with a sphere-like shape (Figure 7a). The diameter of the spheres is about 20 nm. At 40 °C nanorods and nanospheres with several pores were clearly observed (Figure 7b); the size of the nanospheres prepared at 40 °C is larger compared with those prepared at 25 °C, due to agglomeration of the little nanoparticles. When the reaction temperature rose to 60 °C, highly porous In_2O_3 nanorods with a diameter and length of about 90 and 500 nm, respectively, were obtained (see Figure 6a). As the temperature further rose to 80 °C, nanorods became shorter and self-assembled into ordered bundles through van der Waals interactions (Figure 7c).[37] 60 °C is a suitable temperature for preparing mesoporous In_2O_3 nanorods. As we know, the aggregation and phase behavior in water of triblock copolymers of poly(oxyethylene)-poly(oxypropylene)- poly-(oxyethylene) was related to critical micelle concentration (CMC).[38] However, The CMC values for triblock copolymers decrease strongly with increasing temperature. When triblock copolymers solution has relatively low temperature, it forms spherical micelles. As the temperature increases the shape of micelle changes to cubic and then to claviform. Therefore, when the reactive temperature rose from 25 to 80 °C, the morphology of In_2O_3 changed from nanospheres to nanorods.

Influence of the Dosage of $InCl_3$ on the Architecture. Figure 8 shows TEM micrographs of In_2O_3 prepared with different dosages of $InCl_3$. When the dosage of $InCl_3$ increased from 0.005 mol to 0.010 mol, the ratio of length to diameter increased from about 3.7 to 8.9, and the porosity increased. When the dosage of $InCl_3$ rose to 0.015 mol, shorter and thicker nanorods were obtained. Experimental results showed that 0.01 mol of $InCl_3$ was suitable for forming highly porous nanorods with the maximum ratio of length to diameter.

Influence of the pH Value on the Morphology. Figure 9 presents the TEM micrographs of In_2O_3 at different pH values. The results showed that when pH < 6.4, the samples were nanorods without pores. After the pH was increased to 6.4, highly porous nanorods consisting of interconnected nanocrystallites of ~20 nm could be observed in the products. When

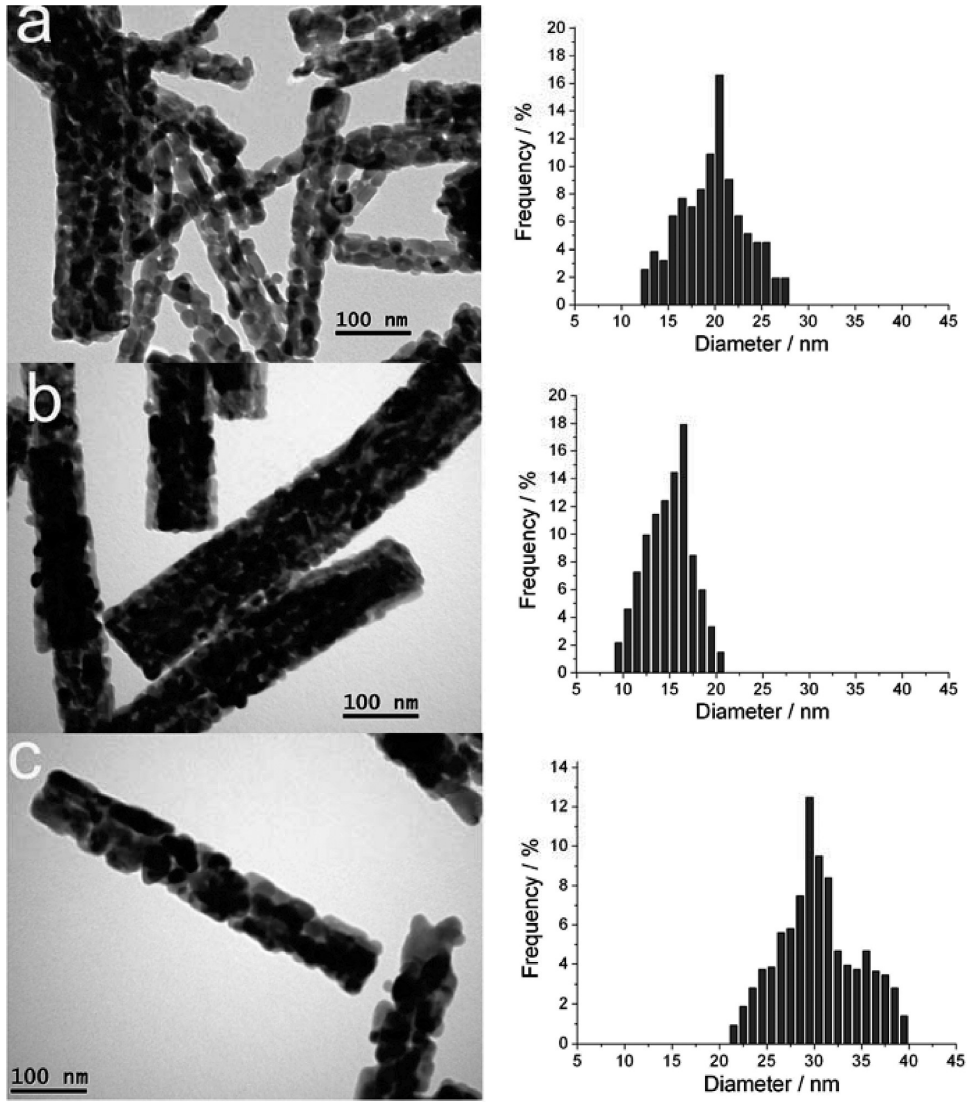

Figure 6. TEM image and size distribution of In_2O_3 obtained under different quantities of PE6800. (a) 1.0 g; (b) 0.5 g; (c) 1.5 g.

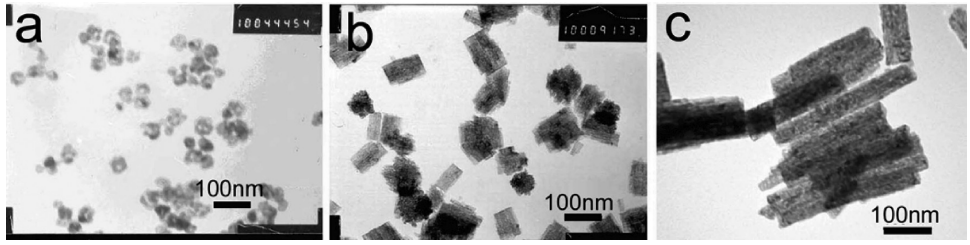

Figure 7. TEM image of In_2O_3 obtained under different reaction temperatures. (a) 25 °C; (b) 40 °C; (c) 80 °C.

the pH rose to 7.5, the samples were nanorods without pores and agglomerated strongly.

3.4. Gas-Sensing Properties of Gas Sensor. The mesoporous In_2O_3 nanorods showed excellent gas-sensing properties to dilute ethanol; it could detect ethanol down to 500 ppb with a response value of about 1.71. The response and the recovery time were 6 and 8 s, respectively. The response and variation in sensitivity of In_2O_3 sensors with ethanol concentration ranging from 0.5 to 1000 ppm are shown in Figure 10. As shown, the response to 50 ppm ethanol could reach 7.32. In addition, the reversibility and repeatability were also good. When the ethanol concentration was in the range of 0.5−1000 ppm, the logarithm

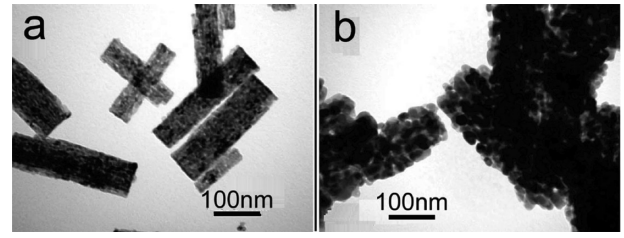

Figure 8. TEM image of In_2O_3 obtained under dosage of $InCl_3$. (a) 0.005 mol; (b) 0.015 mol.

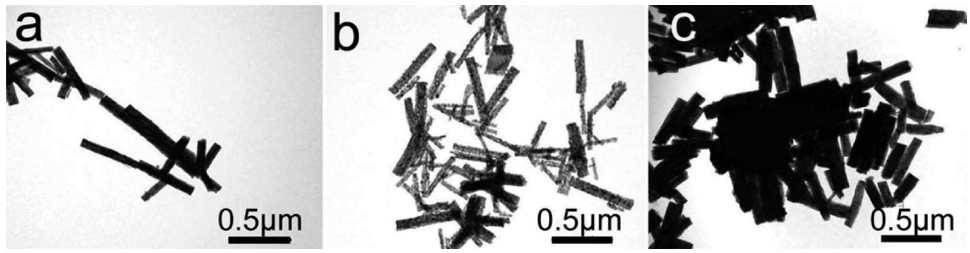

Figure 9. TEM image of In_2O_3 obtained under different pH values. (a) pH = 5.0; (b) pH = 6.4; (c) pH = 7.5.

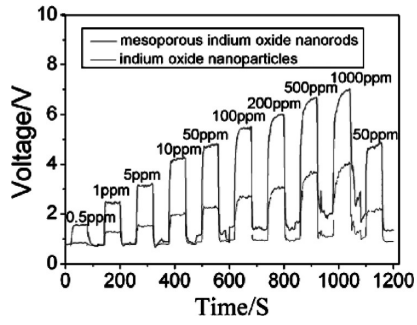

Figure 10. Typical response curve of mesoporous In_2O_3 nanorods and In_2O_3 nanoparticles sensors to 0.5−1000 ppm ethanol.

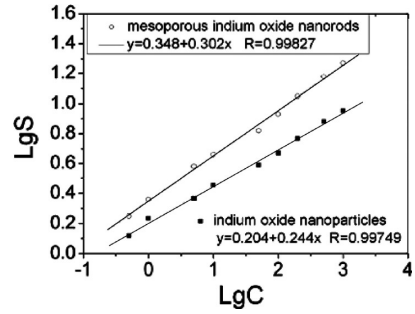

Figure 11. Variation of the sensitivity of mesoporous In_2O_3 nanorods and In_2O_3 nanoparticles sensors with ethanol concentration.

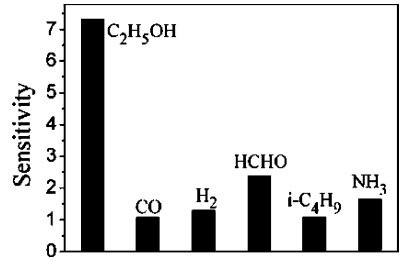

Figure 12. Sensitivity values of the mesoporous In_2O_3 nanorods sensor to different gases of 50 ppm.

of sensitivity showed good linearity with the logarithm of ethanol concentration (Figure 11).

We also measured the response of the sensors to some typical combustible and toxic gases such as CO, H_2, HCHO, i-C_4H_9, NH_3 at 290 °C. The response of mesoporous In_2O_3 nanorods sensors to different gases is shown in Figure 12. The response of different gases was obtained at the same concentration of 50 ppm. As shown in Figure 12, the sensor reponses to CO, H_2, HCHO, i-C_4H_9, NH_3 were low with respect to that obtained for C_2H_5OH. The conventional ethanol sensors, mostly based on SnO_2, ZnO, usually suffer from cross-sensitivity to other gases, though they have rather high sensitivity to ethanol.[39] The sensors based on mesoporous In_2O_3 nanorods showed an obvious advantage in selective detection of ethanol.

In order to examine the influence of the product morphology on its gas-sensing properties to C_2H_5OH, the sample of In_2O_3 particles synthesized without PE6800 was also studied under the same test conditions. As shown in Figure 10 the gas response of the sensor based on mesoporous In_2O_3 nanorods was higher than that of In_2O_3 nanoparticles.

The sensor response is determined mainly by the quantity of active sites on the surface of gas sensors: grain-boundaries or grain-junctions are considered as the active sites and they act positively on the sensor response, whereas secondary grains, in which many grain-boundaries have disappeared during their formation, act negatively on the sensor response.[40,41] A possible reason for the different gas-sensing properties between In_2O_3 nanoparticles and mesoporous In_2O_3 nanorods is that the as-synthesized mesoporous In_2O_3 nanorods are composed of many small well-aligned nanoparticles and many nanoparticles/nanoparticles grain-boundaries could be formed. In contrast, In_2O_3 nanoparticles prepared without PE6800 are not only in large grain size but also have serious agglomeration which was typical large secondary grains with a fewer amount of grain-boundaries. So the gas response of the sensor based on mesoporous In_2O_3 nanorods was higher than that of In_2O_3 nanoparticles.

4. Conclusions

In summary, mesoporous In_2O_3 nanorods have been successfully synthesized by a simple sol−gel method with three block copolymer PE6800 controlling their morphology and indium chloride as a precursor. TEM image reveals that the synthesized In_2O_3 materials had highly porous structure consisting of interconnected nanocrystallites of about 20 nm in size. In our experiments, the concentration and kinds of surfactants, the dosage of $InCl_3 \cdot 4H_2O$, reaction temperature, and pH values played important roles in governing the morphology of In_2O_3. The gas sensitivity results showed that mesoporous In_2O_3 nanorods were very sensitive to dilute ethanol. It could detect 500 ppb C_2H_5OH at about 290 °C with a reponse value of about 1.71 and the response and the recovery time were 6 and 8 s, respectively.

Acknowledgment. The authors thank Qiang Li of Instrumental Analysis and Research Center in Shanghai University for his technical assistance. This work is supported by the Shanghai Natural Science Foundation (07ER14039) and Leading Academic Discipline Project of Shanghai Municipal Education Commission (J50102).

References

(1) Kresge, C. T.; Leonwicz, M. E.; Roth, W. J.; Vartuli, J. C.; Beck, J. S. *Nature* **1992**, *359*, 710.

(2) Kisler, J. M.; Dahler, A.; Stevens, G. W.; Connor, J. O. *Microporous Mesoporous Mater.* **2001**, *44*, 769.
(3) He, X.; Antoneili, D. *Angew. Chem., Int. Ed.* **2001**, *41*, 214.
(4) Chae, W. S.; Kim, Y. R.; Jung, J. S. J. *Phys. Chem B.* **2003**, *107*, 1585.
(5) Parala, H.; Winkler, H.; Kolbe, M.; Wohlfart, A.; Fischer, R. A.; Schmechel, R.; Seggen, H. V. *Adv. Mater.* **2000**, *12*, 1050.
(6) Wager, T.; Waitz, T.; Roggenbuck, J.; Froba, M.; Kohl, C. D.; Tiemann, M. *Thin Solid Films* **2007**, *515*, 8360.
(7) Shimizu, Y.; Jono, A.; Hyodo, T. *Sens. Actuator B.* **2005**, *108*, 56.
(8) Page, M. G.; Nassif, N.; Borner, H. G.; Antonietti, M.; Colfen, H. *Cryst. Growth Des.* **2008**, *8*, 1792.
(9) Lyu, Y. Y.; Yi, S. H.; Shon, J. K.; Chang, S.; Pu, L. S.; Lee, S. Y.; Yie, J. E.; Char, K.; Stucky, G. D.; Kim, J. M. *J. Am. Chem. Soc.* **2004**, *126*, 2310.
(10) Lu, Q.; Gao, F.; Komaeneni, S.; Mallouk, T. E. *J. Am. Chem. Soc.* **2004**, *126*, 8650.
(11) Smith, R. L.; Collins, S. D. *J. Appl. Phys.* **1992**, *71*, R1−22.
(12) Baughman, R. H.; Zakhidov, A. A.; Hee, W. A. *Science* **2002**, *297*, 787.
(13) Pan, Z. W.; Dai, Z.R.; Wang, Z. L. *Science* **2001**, *291*, 1947.
(14) Wang, Y. D.; Ma, C. L.; Sun, X. D.; Li, H. D. *Inorg. Chem. Commun.* **2002**, *5*, 751.
(15) Shi, W. S.; Zheng, Y. F.; Wang, N.; Lee, C. S.; Lee, S. T. *Adv. Mater.* **2001**, *13*, 591.
(16) Morales, A. M.; Lieber, C. M. *Science* **1998**, *279*, 208.
(17) Liu, S. W.; Yue, J.; Gedanken, A. *Adv. Mater.* **2001**, *13*, 656.
(18) Bellingham, J. R.; Mackenize, A. P.; Philips, W. A. *Appl. Phys. Lett.* **1991**, *58*, 2506.
(19) Gordon, R. G. *MRS. Bull.* **2000**, 52.
(20) Hambergend.; Granquist., C. G. *J. Appl. Phys.* **1996**, *60*, R123−60.
(21) Xu, J. Q.; Wang, X. H; Li, C. *Electrochem. Solid-State Lett.* **2006**, *9*, 53.
(22) Yang, J.; Li, C. X.; Quan, Z. W.; Kong, D. Y.; Zhang, X. M.; Yang, P. P.; Lin, J. *Cryst. Growth Des.* **2008**, *8*, 695.
(23) Arun, N.; Xu, H. F.; Narayan, P.; Myeongseob, K.; Peng, X. G. *J. Am. Chem. Soc.* **2006**, *128*, 10310.
(24) Hao, Y. F.; Meng, G. W.; Ye, C. H.; Zhang, L. D. *Cryst. Growth Des.* **2005**, *5*, 1617.
(25) Zhu, H.; Wang, X. L.; Yang, F.; Yang, X. R. *Cryst. Growth Des.* **2008**, *8*, 950.
(26) Xu, J. Q.; Chen, Y. P.; Pan, Q. Y.; Cheng, Z. X.; Dong, X. W. *Nanotechnology* **2007**, *18*, 115615.
(27) Gao, T.; Wang, T. H. *J. Cryst. Growth* **2006**, *290*, 660.
(28) Gurlo, A.; Barsan, N.; Weimar, U.; Ivanovskaya, M.; Taurion, A.; Siciliano, P. *Chem. Mater.* **2003**, *15*, 4377.
(29) Atashbar, M. Z.; Gong, B.; Sun, H. T.; Wlodarski, W.; Lamb, R. *Thin Solid Films* **1999**, *354*, 222.
(30) Bianchi, S.; Comini, E.; Ferroni, M.; Faglia, G.; Vomiero, A.; Sberveglieri, G. *Sens. Actuators B.* **2006**, *118*, 204.
(31) Ivanonskaya, M.; Gurlo, A.; Bogdanov, P. *Sens. Actuators B.* **2001**, *77*, 264.
(32) Mccue, J. T.; Ying, J. Y. *Chem. Mater.* **2007**, *19*, 1009.
(33) Zhan, Z. L.; Jiang, D. G.; Xu, J. Q. *Mater. Chem. Phys.* **2005**, *90*, 250.
(34) Chu, X. F.; Wang, C. H.; Jiang, D. L.; Zheng, C. M. *Chem. Phys. Lett.* **2004**, *39*, 461.
(35) Zhu, H.; Wang, X. L.; Yang, F.; Yang, X. R. J. *Cryst. Growth Des.* **2008**, *8*, 955.
(36) Yin, M.; Gu, Y.; Kuskovsky, I. L.; Andelman, T.; Zhu, Y.; Neumark, G. F.; O′Brien, S. *J. Am. Chem. Soc.* **2004**, *126*, 6206.
(37) Wang, Y. L.; Jiang, X. C.; Xia, Y. N. *J. Am. Chem. Soc.* **2003**, *125*, 16176.
(38) Wanka, G.; Hoffmann, H.; UIbricht, W. *Macromolecules.* **1994**, *27*, 4145.
(39) Zhang, T. S.; Hing, P.; Li, Y.; Zhang, J. C. *Sens. Actuators B.* **1999**, *60*, 208.
(40) Shimizu, Y.; Hyodo, T.; Egashira, M. *Catal. Surv. Asia* **2004**, *8*, 127.
(41) Hyodo, T.; Nishida, N.; Shimizu, Y.; Egashira, M. *Sens. Actuators B.* **2002**, *83*, 209.

CG8007238